ACS OMEGA

Open Access

http://pubs.acs.org/journal/acsodf

Article

Photocatalytic Desulfurization of Thiophene with Chevrel Phase $Ni_2Mo_6S_8$ Synthesized by SHS

Milind Pawar, Anthony Annerino,* Jacob Shell, and Pelagia-Irene Gouma

Cite This: *ACS Omega* 2024, 9, 33935−33940

Read Online

ACCESS | Metrics & More | Article Recommendations | Supporting Information

ABSTRACT: The Chevrel phase compounds $Cu_4Mo_6S_8$, $Ni_2Mo_6S_8$, and $Fe_2Mo_6S_8$, synthesized by self-propagating high temperature synthesis, were evaluated as photocatalysts for visible light photocatalytic desulfurization. Investigations began with reflectance measurements from which absorbance spectra were calculated using the Kubelka−Munk transformation. The absorbance data was then used to create Tauc plots to find the direct and indirect bandgaps of the Chevrel phase compounds. Bandgaps were found to be no more than the 1.74 eV for $Ni_2Mo_6S_8$, so it was selected for further study because this bandgap suggests it will use the sun's emission spectrum better than the other materials studied here. Photocatalytic desulfurization experiments studied the concentration of thiophene mixed into *n*-octane with and without exposure to $Ni_2Mo_6S_8$ with and without light exposure because of the relative difficulty of removing thiophenes from liquid fossil fuels by the industry standard hydrodesulfurization process. Ultraviolet−visible spectroscopy was used to analyze chemical changes in the thiophene-octane solution. Spectroscopic results demonstrate that the thiophene was effectively removed by exposure to $Ni_2Mo_6S_8$ and visible light together but not by exposure to $Ni_2Mo_6S_8$ or visible light alone. Multiple tests with the same $Ni_2Mo_6S_8$ sample demonstrate that the material is reusable as a catalyst for photocatalytic desulfurization. The proposed mechanism results in the release of SO_x species, which may be controlled and captured if separated from fossil fuels in bulk during industrial processing in contrast to their uncontrolled release as vehicle fuel exhaust. Controlled generation and collection of these species can allow for further processing into elemental sulfur in the same way that H_2S released by standard hydrodesulfurization is processed into elemental S.

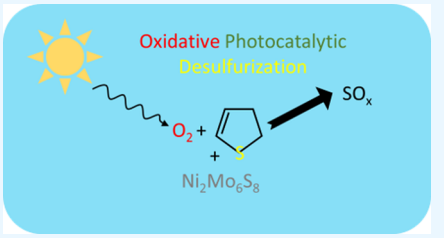

1. INTRODUCTION

Removing sulfurous compounds from fossil fuels before they can be burned and released as SO_2 is a critical process in protecting the environment from further damage from greenhouse gases.[1−4] Hydrodesulfurization is the most widely used method for removing sulfurous compounds from crude oil before processing into consumer products such as gasoline and diesel fuel.[5−7] Hydrodesulfurization works well in converting thiols and disulfides into H_2S, from which the elemental S can later be reclaimed for further use, but this process is much less effective at converting thiophenes into H_2S even when run at elevated temperatures and pressures.

Energy-efficient photocatalytic desulfurization has previously been reported using a variety of catalysts, but no work has been presented with Chevrel phase compounds (CPCs) for photocatalytic oxidative desulfurization.[8−10] CPCs are ternary metal chalcogenides following the general chemical formula $M_xMo_6X_8$ (where M is a ternary cation, and X is S, Se, or Te), and they form crystal structures based on building blocks composed of Mo octahedrons superimposed onto X8 cubes with wide channels between them where the M species reside.[11,12] Over the years, many applications have been envisioned for CPCs. Early electrocatalysis applications including hydrodesulfurization and hydrogen evolution reaction catalysis have been investigated, and more recent investigations include CO_2 reduction and O_2 reduction as detailed in the recent review by Zhang et al.[12−15] In parallel, research has been ongoing for years to investigate the superconducting properties of CPCs, especially their high critical field, as described in the holistic review by Peña.[16−18] Still others have investigated CPCs as thermoelectric materials.[19,20] CPCs have also been investigated as possible cathodes, first for Li-ion batteries, then for Mg-ion batteries, and most recently for Al-ion batteries that hope to realize the theoretical prediction of tripling or quadrupling the energy density of contemporary Li-ion batteries.[21,22]

However, CPCs have been limited in use due to slow and inefficient synthesis methods.[11,23−26] A recent publication by this group highlights new progress made in synthesizing CPCs by self-propagating high temperature synthesis (SHS).[11] The primary merit of this SHS method is the rapid synthesis of $Cu_4Mo_6S_8$, $Ni_2Mo_6S_8$, and $Fe_2Mo_6S_8$ with high conversion of precursor materials into product materials.

Received: May 2, 2024
Revised: July 15, 2024
Accepted: July 18, 2024
Published: July 26, 2024

Eligibility of a material as a photocatalyst depends on that material's band gap; visible light photocatalysts have band gaps in the range of light emitted from the sun.[27] Past work suggests that other CPCs have band gaps in the range required for photocatalysis.[28−30] A fast and high yield synthesis of a visible light activated photocatalyst that desulfurizes fuel through removal of thiophene would be of large interest to fossil fuel companies and environmentalists alike. Such a material would fill the gap left by hydrodesulfurization in an economic and convenient fashion, thus inspiring this investigation of the band gap and photocatalytic activity of CPCs synthesized by SHS.

2. EXPERIMENTAL PROCEDURES

2.1. Material Synthesis and Characterization. The Chevrel phase compounds were synthesized by mixing Mo (SkySpring Materials) and MoS_2 (Climax Molybdenum) powders with elemental powders of Ni, Fe, and Cu (SkySpring Materials) in the stoichiometric ratio of xM:2Mo:4MoS_2. Here, M is Ni, Fe, or Cu and x is 2, 2, or 4, respectively. These mixtures were pressed into pellets and then vacuum encapsulated into a quartz reaction vessel. To activate the SHS reaction, the reaction vessel was held in a tube furnace set to 1050 °C for 10 min. Product phase identification was accomplished using X-ray diffraction and selected area electron diffraction with the X-ray diffraction (XRD) spectra of the SHS $Cu_4Mo_6S_8$, $Ni_2Mo_6S_8$, and $Fe_2Mo_6S_8$ respectively matching ICSD files 628442, 602930, and 14069. Representative XRD spectra and scanning electron microscope (SEM) images of these samples were part of another published work by the authors and are included here in the Supporting Information as Figures S1 and S2 with permission from the publisher of that other article.[11]

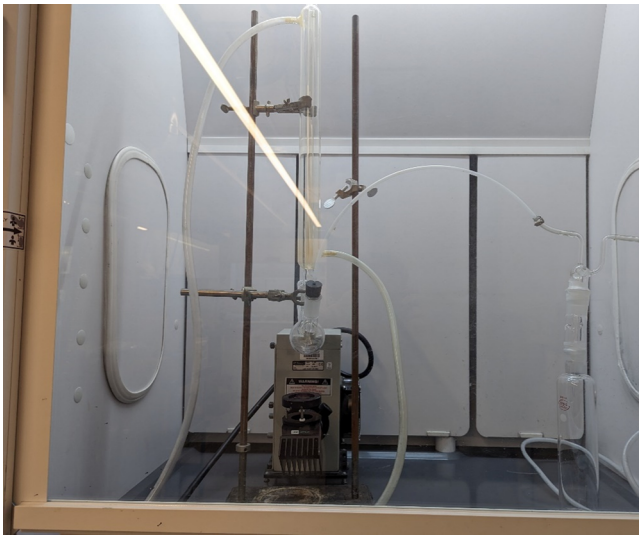

Figure 1. Photocatalytic desulfurization apparatus.

2.2. Reflectance Measurements and Bandgap Calculations. Using an Ocean Optics HR-4000 spectrophotometer with Ocean Optics DH-2000 light source in diffuse reflectance mode, ultraviolet−visible (UV−vis) spectroscopy was conducted on each of the CPCs discussed above. These reflectance spectra were then converted into absorbance spectra using the Kubelka−Munk transformation shown in eq 1[31,32]

$$F(R_\infty) = \frac{K}{S} = \frac{(1 - R_\infty)^2}{2R_\infty} \quad (1)$$

where R_∞ is the reflectance of the sample divided by the standard reflectance (i.e., the reflectance of an infinitely thick specimen), K is the absorption coefficient, and S is the scattering coefficient. The standard reflectance was taken to be 100 in this study. From there, a direct band gap energy and an indirect band gap energy was estimated via the Tauc estimation method for each material, displayed by the relationship in eq 2[32,33]

$$(\alpha \cdot h\nu)^{1/\gamma} = B(h\nu - E_g) \quad (2)$$

where h is Planck's constant, ν is the light's frequency, E_g is the bandgap, and B is a constant. The γ value varies as either 0.5 or 2 for direct or indirect bandgap calculations, respectively.[32] To ensure consistency and accuracy in the calculation of the bandgaps, GapExtractor software was used to automate the process of calculating the estimated band gaps.[34,35]

2.3. Photocatalytic Desulfurization Experiments. First, the composition of the MF for the photocatalytic desulfurization experiments was selected. This process started with collecting UV−vis absorbance spectra of thiophene solutions in *n*-octane with concentrations of 20, 100, and 500 ppm using a quartz cuvette and the aforementioned Ocean Optics equipment, now operated in transmission mode. After selecting 100 ppm thiophene in *n*-octane as the MF for use in the following tests, experiments were performed to verify that the thiophene concentration was not changed by exposure to either visible light or $Ni_2Mo_6S_8$ alone. The first of these tests involved exposing the as-prepared MF to the Hg lamp emission for 2 h without exposure to $Ni_2Mo_6S_8$. The second of these tests involved combining 10 mL of MF with 200 mg of $Ni_2Mo_6S_8$ in a sealed container that was wrapped entirely in aluminum foil and letting it sit for 2 h.

After collecting absorbance UV−vis spectra to document the interactions of the MF with light and $Ni_2Mo_6S_8$ alone, tests were conducted to investigate possible photocatalytic activity achieved by simultaneously exposing the MF to light and $Ni_2Mo_6S_8$. These tests started with combining 200 mg of $Ni_2Mo_6S_8$ and 10 mL of MF in the reaction vessel then allowing the mixture to equilibrate in the dark for an hour. Next, the mixture was exposed to the filtered Hg lamp emission for 2 h. Finally, a sample of the MF was removed from the reaction vessel for UV−vis absorbance spectroscopy to check the remaining thiophene content. Intensity of the previously established main thiophene peak in the range 230−245 nm was taken the indicator of changes in the thiophene content after the photocatalytic treatment.[36] Catalytic reusability was tested by running 2 of these tests with the same 200-mg catalyst sample in 2 separate 10 mL MF samples where the catalyst sample was dried between successive tests.

Desulfurization was monitored by absorbance UV−vis spectroscopy using the same Ocean Optics HR-4000 spectrophotometer and Ocean Optics DH-2000 light source described previously, now operated in transmission mode. All absorbance spectra were collected using a quartz cuvette, and a scan of the empty quartz cuvette was used as the calibration standard spectrum. This procedure was done for all UV−vis measurements taken of liquid samples in this study.

The experimental photocatalytic desulfurization apparatus was composed of a three-headed round-bottom glass flask

https://doi.org/10.1021/acsomega.4c04213
ACS Omega 2024, 9, 33935−33940

fitted with a reflux condenser on one of its openings and a bleach trap affixed to the top of the condenser. Cool water was run through the condenser, and air was bubbled through water into the flask through one of the other openings. During experiments, the flask was either wrapped in aluminum foil to block out all light or suspended 10 cm above a 125 W Hg lamp fitted with a UV light cutoff filter. The test mixture held in the flask was a model fuel (MF) composed of 100 ppm thiophene in *n*-octane which was meant to mimic commercial gasoline. Figure 1 displays the testing apparatus.

3. RESULTS AND DISCUSSION

3.1. CPC Band Gaps. Figure 2a displays the measured reflectance data for each of the CPCs. Using the Kubelka–Munk transformation shown in eq 1, those reflectance spectra were converted into absorbance spectra.[31,32] The resultant absorbance spectra are displayed in Figure 2b.

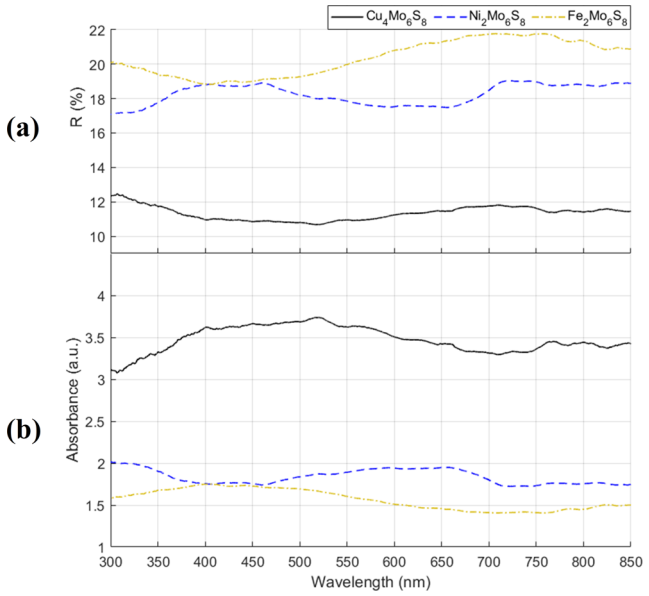

Figure 2. (a) Experimental reflectance spectra and (b) calculated absorbance spectra for each CPC studied here.

From this absorbance data, the Tauc method was used to calculate the direct and indirect bandgaps.[32,33] The GapExtractor program determined the bandgaps using a segmentation routine to identify the linear regions in the Tauc plots to be extrapolated for band gap estimation.[34,35] Figure 3 presents the direct and indirect band gap Tauc plots for $Ni_2Mo_6S_8$ as generated by GapExtractor using eq 2. Figure S1 in the supplementary document displays the analogous Tauc plots for $Cu_4Mo_6S_8$ and $Fe_2Mo_6S_8$. The band gaps of all 3 CPCs studied

Table 1. Direct and Indirect Band Gaps of $Ni_2Mo_6S_8$, $Cu_4Mo_6S_8$, and $Fe_2Mo_6S_8$

material	direct bandgap (eV)	indirect bandgap (eV)
$Ni_2Mo_6S_8$	1.74	1.73
$Cu_4Mo_6S_8$	1.67	1.67
$Fe_2Mo_6S_8$	1.63	1.63

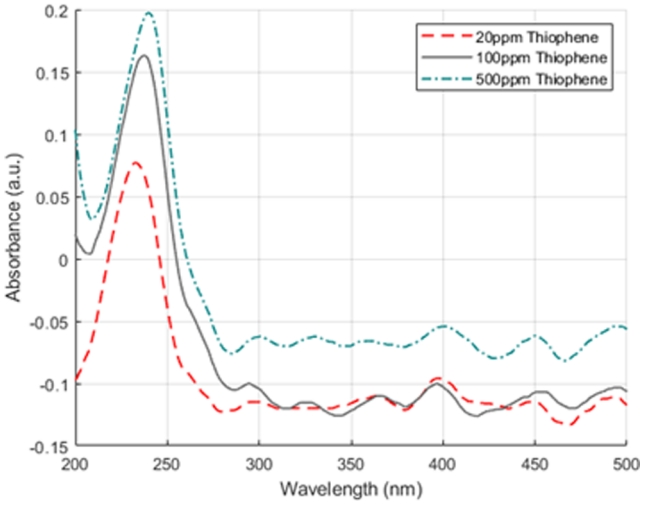

Figure 4. Absorbance spectra of 20, 100, and 500 ppm thiophene in *n*-octane.

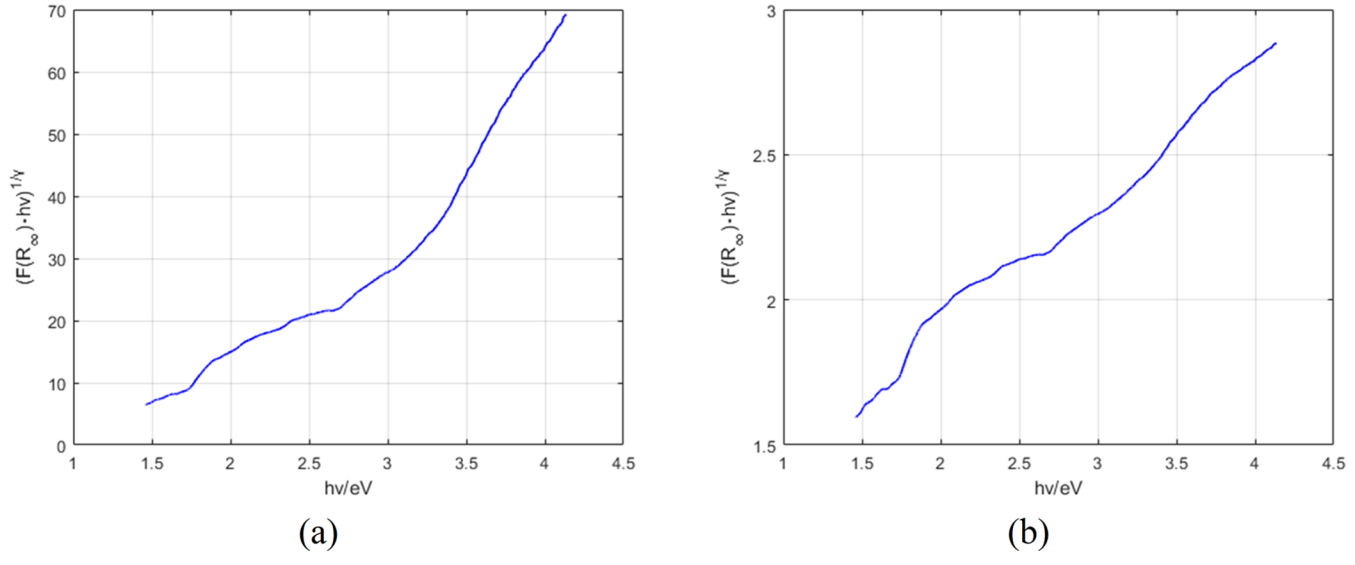

Figure 3. (a) Direct band gap Tauc plot and (b) indirect band gap Tauc plot for $Ni_2Mo_6S_8$.

https://doi.org/10.1021/acsomega.4c04213
ACS Omega 2024, 9, 33935−33940

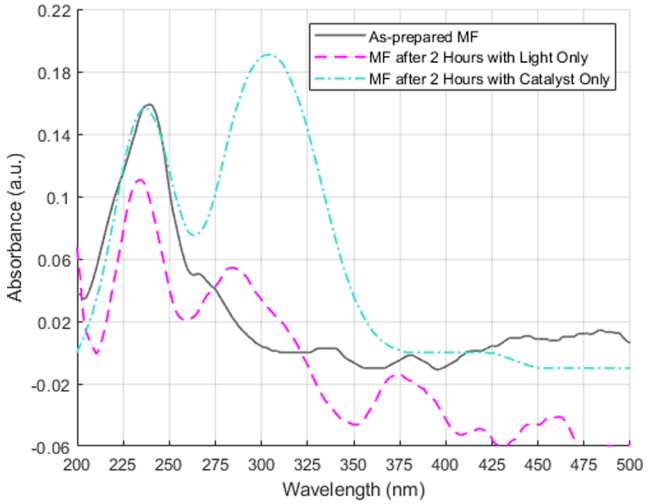

Figure 5. Absorbance spectra of the MF in the as-prepared state and after 2 h of exposure to light and $Ni_2Mo_6S_8$ separately.

here were also estimated by manually following the convention of extrapolating the linear region of the Tuac plot and estimating the band gap as the x-intercept of that extrapolation to verify that the GapExtractor results are valid. These band gap values are displayed in Table 1.

From these results, $Ni_2Mo_6S_8$ was selected for photocatalytic desulfurization experiments. The direct bandgap of 1.74 eV in $Ni_2Mo_6S_8$ will make best use of the sun's emission spectrum in electron−hole pair generation, making it the most attractive option for these experiments.[37] However, the other 2 materials still show significant promise as photocatalysts that simply will not be able to use as much of the sun's full emission spectrum.

3.2. Determining the Model Fuel Composition. Figure 4 shows the absorbance spectra of 3 candidate concentrations of thiophene in *n*-octane. Note the main thiophene peak in the range 230−245 nm; the height of this peak was the metric used for the comparisons presented in this manuscript. The difference between the 100 and 20 ppm thiophene spectra was significantly larger than that between the 500 and 100 ppm spectra, inspiring the decision to use the 100 ppm thiophene in *n*-octane as the MF because differences in thiophene concentration after desulfurization would be most readily detected at this concentration. Going forward, this 100 ppm thiophene in *n*-octane is the as-prepared MF.

3.3. Photocatalytic Desulfurization of the Model Fuel. Figure 5 demonstrates that exposure to either light or $Ni_2Mo_6S_8$ alone did not eliminate the main thiophene peak. However, there was some slight decrease in the main thiophene peak after 2 h of light exposure. This detail was noted and considered during the analysis of the following photocatalytic desulfurization experiments. The new peak in the "MF after 2 h with catalyst only" curve was attributed to the presence of the $Ni_2Mo_6S_8$ in the MF.

Figure 6 displays the results of sequential photocatalytic desulfurization experiments where the same 200-mg photocatalyst sample was used to desulfurize 2 different MF samples. Note the major reduction in the thiophene main peak intensity. Furthermore, similar performance was observed in the second round of using the same 200-mg sample of $Ni_2Mo_6S_8$, indicating that the observed phenomenon is repeatable and supporting the assertion that this phenomenon is catalytic in nature rather than reliant upon consuming the $Ni_2Mo_6S_8$ as part of some other chemical reaction. This total elimination of the thiophene peak from the UV−vis spectra is itself not groundbreaking since others have reported nearly or totally removing thiophene and its derivatives in similar experiments with other photo-oxidative catalysts. What makes this result comparatively noteworthy is the relative procedural simplicity of this material's synthesis process in comparison with the multistep processes reported alongside these other investigations of composite Mn_3O_4/Ag_2WO_4, composite graphene oxide/MoS_2, and mesoporous graphitic carbon nitride.[8−10]

The observed photocatalytic desulfurization by $Ni_2Mo_6S_8$ is attributed to a photo-oxidative mechanism driven by the presence of oxygen and moisture supplied by bubbling air through water into the MF during the experiments. The proposed mechanism starts with photonic excitation of electrons into the conduction band of the $Ni_2Mo_6S_8$ photocatalyst, enabled by its relatively narrow band gap. Photoexcitation generates valence band holes (h_{VB}^+) and conduction band electrons (e_{CB}^-). These species then generate oxygen radicals ($^\bullet O_2^-$) and hydroxide radicals ($^\bullet OH$) from

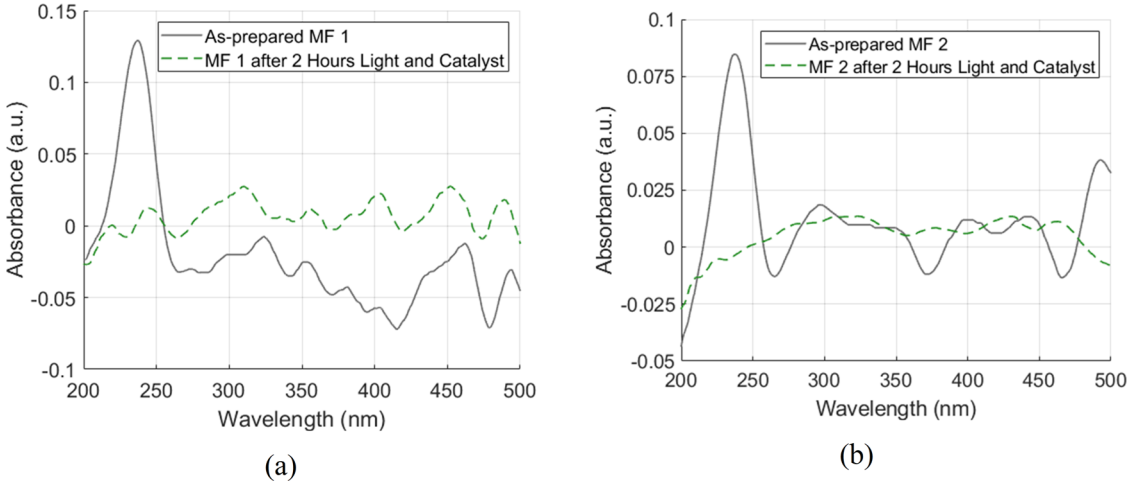

Figure 6. (a) Absorbance spectra of MF before and after photocatalytic desulfurization with a fresh catalyst sample and (b) absorbance spectra of a second MF sample before and after photocatalytic desulfurization with the same catalyst sample reused.

https://doi.org/10.1021/acsomega.4c04213
ACS Omega 2024, 9, 33935−33940

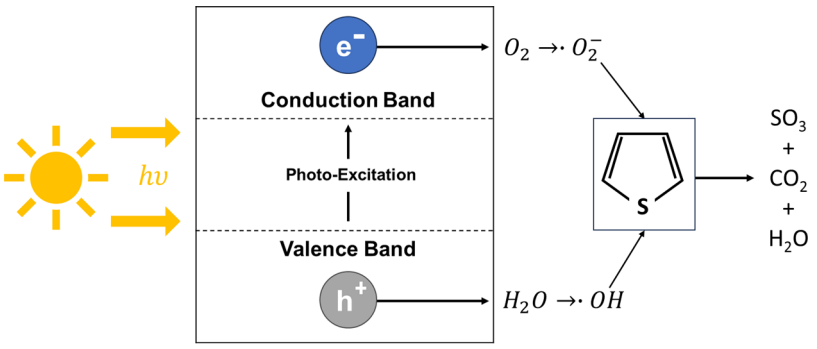

Figure 7. Schematic of proposed $Ni_2Mo_6S_8$-catalyzed photo-oxidative desulfurization mechanism.

oxygen and water molecules adsorbed on the surface of the $Ni_2Mo_6S_8$ photocatalyst then follows. These radicals then attack thiophene molecules adsorbed on the $Ni_2Mo_6S_8$ surface, and the sulfur is discharged as SO_3 while the rest of the thiophene atoms are converted to CO_2 and H_2O following the same mechanism for the photo-oxidative desulfurization of thiophene and thiophene derivatives by other photocatalysts published elsewhere.[8−10] This mechanism is illustrated by reactions 3−6 below.

$$h\nu + Ni_2Mo_6S_8 \rightarrow h^+_{VB} + e^-_{CB} \quad (3)$$

$$h^+_{VB} + H_2O_{ads} \rightarrow {}^{\bullet}OH \quad (4)$$

$$e^-_{CB} + O_{2ads} \rightarrow {}^{\bullet}O_2^- \quad (5)$$

$${}^{\bullet}OH + C_4H_4S + {}^{\bullet}O_2^- \rightarrow CO_2 + H_2O + SO_3 \quad (6)$$

While the whole point of desulfurizing fossil fuels is to prevent the release of damaging greenhouse gases like CO_2 and SO_3, the controlled creation and subsequent collection of these species in a plant is preferable to the uncontrolled release of them in vehicle exhaust. Controlled generation and collection can allow for further processing into elemental sulfur like the gaseous H_2S released by standard hydrodesulfurization. This proposed mechanism is illustrated in Figure 7.

4. CONCLUSIONS

The CPC $Ni_2Mo_6S_8$ synthesized by SHS from elemental Ni, elemental Mo, and MoS_2 has been proven to function as a photocatalyst for photo-oxidative desulfurization of an *n*-octane model fuel containing 100 ppm of thiophene. It was demonstrated that the large drop in thiophene concentration is not solely due to either the light exposure itself or light-independent interactions with the $Ni_2Mo_6S_8$ photocatalyst. $Ni_2Mo_6S_8$ demonstrated the ability to be reused as a photocatalyst for this photo-oxidative desulfurization, as repeated runs with the same photocatalyst sample demonstrated similar photocatalytic efficacy. The other CPCs $Cu_4Mo_6S_8$ and $Fe_2Mo_6S_8$ which can be synthesized by the same method also show promise for photocatalysis applications after finding that their band gap energies are like that of the $Ni_2Mo_6S_8$.

■ ASSOCIATED CONTENT

Supporting Information

The Supporting Information is available free of charge at https://pubs.acs.org/doi/10.1021/acsomega.4c04213.

Experimental and reference XRD spectra of reported Chevrel phase compounds (Figure S1); SEM images of reported Chevrel phase compounds (Figure S2); and direct and indirect band gap Tauc plots for $Cu_4Mo_6S_8$ and $Fe_2Mo_6S_8$ (Figure S3) (PDF)

■ AUTHOR INFORMATION

Corresponding Author

Anthony Annerino − *Department of Materials Science and Engineering, The Ohio State University, Columbus, Ohio 43210, United States;* orcid.org/0000-0002-7435-6793; Email: Annerino.2@osu.edu

Authors

Milind Pawar − *Department of Materials Science and Engineering, The Ohio State University, Columbus, Ohio 43210, United States;* Present Address: HCL America, Inc., Redmond, Washington 98052, United States

Jacob Shell − *Department of Materials Science and Engineering, The Ohio State University, Columbus, Ohio 43210, United States;* orcid.org/0009-0004-1583-5294

Pelagia-Irene Gouma − *Department of Materials Science and Engineering, The Ohio State University, Columbus, Ohio 43210, United States; Department of Mechanical and Aerospace Engineering, The Ohio State University, Columbus, Ohio 43210, United States*

Complete contact information is available at: https://pubs.acs.org/10.1021/acsomega.4c04213

Author Contributions

Conceptualization, M.P. and P.-I.G.; methodology, M.P.; software, M.P.; validation, M.P. and P.-I.G.; formal analysis, M.P.; investigation, M.P.; resources, P.-I.G.; data curation, M.P. and A.A.; writing—original draft preparation, M.P. and A.A; writing—review and editing, A.A. and J.S.; visualization, A.A. and J.S.; supervision, P.-I.G.; project administration, P.-I.G.; funding acquisition, P.-I.G. All authors have read and agreed to the published version of the manuscript.

Notes

The authors declare no competing financial interest.

■ ACKNOWLEDGMENTS

The authors thank the Edward Orton Jr., Ceramic Foundation for financial support that allowed this research.

■ ABBREVIATIONS

SHS, self-propagating high-temperature synthesis; UV−vis, ultraviolet−visible; CPC, Chevrel phase compound; MF, model fuel

■ REFERENCES

(1) Zaid, H. F. M.; Kait, C. F.; Mutalib, M. I. A. Photooxidative−extractive deep desulfurization of diesel using Cu−Fe/TiO2 and eutectic ionic liquid. *Fuel* **2015**, *156*, 54−62.

(2) Markel, E. J.; Burdick, S. E.; Leaphart, M. E.; Roberts, K. L. Synthesis, characterization, and thiophene desulfurization activity of unsupported Γ-MO2N macrocrystalline catalysts. *J. Catal.* **1999**, *182* (1), 136−147.

(3) Schoofs, G. R.; Preston, R. E.; Benziger, J. Adsorption and desulfurization of thiophene on nickel(111). *Langmuir* **1985**, *1* (3), 313−320.

(4) Moses, P. G.; Hinnemann, B.; Topsøe, H.; Nørskov, J. K. The hydrogenation and direct desulfurization reaction pathway in thiophene hydrodesulfurization over MoS2 catalysts at realistic conditions: A density functional study. *J. Catal.* **2007**, *248* (2), 188−203.

(5) McCarty, K. F. Hydrodesulfurization catalysis by Chevrel phase compounds. *J. Catal.* **1985**, *93* (2), 375−387.

(6) Sawhill, S. J.; Phillips, D.; Bussell, M. E. Thiophene hydrodesulfurization over supported nickel phosphide catalysts. *J. Catal.* **2003**, *215* (2), 208−219.

(7) Satterfield, C. N.; Modell, M.; Mayer, J. F. Interactions between catalytic hydrodesulfurization of thiophene and hydrodenitrogenation of pyridine. *AIChE J.* **1975**, *21* (6), 1100−1107.

(8) Shawky, A.; Mohamed, R. M.; Mkhalid, I. A.; Awwad, N. S.; Ibrahium, H. A. One-pot synthesis of Mn3O4-coupled Ag2WO4 nanocomposite photocatalyst for enhanced photooxidative desulfurization of thiophene under visible light irradiation. *Appl. Nanosci.* **2020**, *10* (5), 1545−1554.

(9) Alhaddad, M.; Shawky, A. Superior photooxidative desulfurization of thiophene by reduced graphene oxide-supported MoS2 nanoflakes under visible light. *Fuel Process. Technol.* **2020**, *205*, No. 106453.

(10) Zhu, Y.; Li, X.; Zhu, M. Mesoporous graphitic carbon nitride as photo-catalyst for oxidative desulfurization with oxygen. *Catal. Commun.* **2016**, *85*, 5−8.

(11) Pawar, M.; Gouma, P. Intercalation-assisted massive phase transformation: The key to SHS synthesis? *J. Am. Ceram. Soc.* **2022**, *105* (12), 7159−7170.

(12) Zhang, W.; Zhang, W.; Tan, J.; et al. Chevrel phases: synthesis, structure, and electrocatalytic applications. *Mater. Chem. Front.* **2023**, *7*, 5500−5518.

(13) McCarty, K. F.; Schrader, G. L. Hydrodesulfurization by reduced molybdenum sulfides: activity and selectivity of Chevrel phase catalysts. *Ind. Eng. Chem. Prod. Res. Dev.* **1984**, *23* (4), 519−524.

(14) Ekman, M.; Anderegg, J. W.; Schrader, G. L. Reduced molybdenum formal oxidation states in hydrodesulfurization catalysis by Chevrel phases. *J. Catal.* **1989**, *117* (1), 246−257.

(15) Naik, K. M.; Sampath, S. Cubic Mo6S8-efficient electrocatalyst towards hydrogen evolution over wide pH range. *Electrochim. Acta* **2017**, *252*, 408−415.

(16) Fischer, Ø. Chevrel phases: Superconducting and normal state properties. *Appl. Phys.* **1978**, *16* (1), 1−28.

(17) Matthias, B. T.; Marezio, M.; Corenzwit, E.; Cooper, A. S.; Barz, H. High-Temperature superconductors, the first ternary system. *Science* **1972**, *175* (4029), 1465−1466.

(18) Peña, O. Chevrel phases: Past, present and future. *Phys. C* **2015**, *514*, 95−112.

(19) Schmidt, A. Investigation of New Chevrel Phase Compounds for Improved Efficiency of Thermoelectric Power Generation Devices. MS Thesis, Cornell University, 2005. https://hdl.handle.net/1813/2119.

(20) Caillat, T.; Fleurial, J.; Snyder, G. J. Potential of Chevrel phases for thermoelectric applications. *Solid State Sci.* **1999**, *1* (7−8), 535−544.

(21) Uchida, T.; Tanjo, Y.; Wakihara, M.; Taniguchi, M. Nickel-Molybdenum sulfide NI2MO6 S 7.9 as the cathode of lithium secondary batteries. *J. Electrochem. Soc.* **1990**, *137* (1), 7−11.

(22) Tong, Y.; Gao, A.; Zhang, Q.; et al. Cation-synergy stabilizing anion redox of Chevrel phase Mo6S8 in aluminum ion battery. *Energy Storage Mater.* **2021**, *37*, 87−93.

(23) Chevrel, R.; Sergent, M.; Prigent, J. Sur de nouvelles phases sulfurées ternaires du molybdène. *J. Solid State Chem.* **1971**, *3* (4), 515−519.

(24) Sergent, M. Sur des Thiomolybdites, des Thiotungstites et des Thiochromites Alcalins. Ph.D. Dissertation, Université de Rennes, 1969. https://www.sudoc.fr/004554086/id.

(25) Espelund, A. W.; Seip, H. M.; Santesson, J.; et al. Some properties of a ternary sulfide Mo-Sn-S. *Acta Chem. Scand.* **1967**, *21*, 839−841.

(26) Chevrel, R.; Sergent, M. Chemistry and Structure of Ternary Molybdenum Chalcogenides. In *Superconductivity in Ternary Compounds I: Structural, Electronic, and Lattice Properties*; Fischer, O.; Maple, L. B., Eds.; Springer, 1982; pp 25−86.

(27) Zanatta, A. R. Revisiting the optical bandgap of semiconductors and the proposal of a unified methodology to its determination. *Sci. Rep.* **2019**, *91*, No. 11225, DOI: 10.1038/s41598-019-47670-y.

(28) Agiorgousis, M. L.; Sun, Y.; West, D.; Zhang, S. Intercalated chevrel phase MO6S8 as a janus material for energy generation and storage. *ACS Appl. Energy Mater.* **2018**, *1* (2), 440−446.

(29) Perryman, J. T.; Hyler, F. P.; Ortiz-Rodríguez, J. C.; Mehta, A.; Kulkarni, A.; Velázquez, J. M. X-ray absorption spectroscopy study of the electronic structure and local coordination of 1st row transition metal-promoted Chevrel-phase sulfides. *J. Coord. Chem.* **2019**, *72* (8), 1322−1335.

(30) Thöle, F.; Wan, L. F.; Prendergast, D. Re-examining the Chevrel phase Mo6S8 cathode for Mg intercalation from an electronic structure perspective. *Phys. Chem. Chem. Phys.* **2015**, *17* (35), 22548−22551.

(31) Kubelka, P.; Munk, F. An article on optics of paint layers. *Z. Technol. Phys.* **1931**, *12593−601*, 259−274.

(32) Makuła, P.; Pacia, M.; Macyk, W. How to correctly determine the band gap energy of modified semiconductor photocatalysts based on UV−VIS spectra. *J. Phys. Chem. Lett.* **2018**, *9* (23), 6814−6817.

(33) Coulter, J.; Birnie, D. P. Assessing TAUC Plot slope Quantification: ZNO Thin films as a model system. *Phys. Status Solidi B* **2017**, *255*, No. 1700393, DOI: 10.1002/pssb.201700393.

(34) Escobedo-Morales, A.; Ruiz-López, I. I.; del Ruiz-Peralta, M.; Tepech-Carrillo, L.; Sánchez-Cantú, M.; Moreno-Orea, J. E. Automated method for the determination of the band gap energy of pure and mixed powder samples using diffuse reflectance spectroscopy. *Heliyon* **2019**, *5* (4), No. e01505.

(35) Morales, A. E.; Ruiz-López, I. GapExtractor v1.0 *Mendeley Data* 2020. DOI: 10.17632/j9ypzmdx5n.1.

(36) Thiophene. In *Handbook of Data on Organic Compounds*; Weast, R.; Grasselli, J., Eds.; CRC Press: Boca Raton, Florida, USA, 1989; Vol. *6*, p 4289.

(37) Seidlitz, H. K.; Thiel, S.; Krins, A.; Mayer, H.Solar Radiation at the Earth's Surface. In *Comprehensive Series in Photosciences*; Elsevier, 2001; Vol. *3*, pp 705−738.

https://doi.org/10.1021/acsomega.4c04213
ACS Omega 2024, 9, 33935−33940